On the Performance of RIS-Assisted Space Shift Keying: Ideal and Non-Ideal Transceivers

Ayse E. Canbilen, *Member, IEEE*, Ertugrul Basar, *Senior Member, IEEE*, and Salama S. Ikki, *Senior Member, IEEE*

***Abstract*— In this study, we present a unifying framework for future reconfigurable intelligent surface (RIS)-assisted space shift keying (SSK) systems; we additionally propose two novel transmission schemes. The key strategies surrounding this concept, namely power-sensing RIS-SSK and partitioned RIS-SSK, grant knowledge of the activated transmitter (Tx) antenna index at the RIS, which, when using SSK, allows us to adjust the reflection phases. The performance of the proposed scheme is investigated in terms of the theoretical average bit error rate (ABER), and the effect of non-ideal transceivers. The performance is then compared to that of a reference RIS-SSK scheme, and a complexity analysis is provided. The obtained results, verified by extensive computer simulations, demonstrate that the partitioned and power-sensing RIS-SSK schemes achieve a higher ABER than the reference one. Moreover, hardware impairments clearly have a critically degrading impact on the system performance for all schemes, and should be carefully taken into account in future communication systems.**

***Index Terms*— Error performance analysis, index modulation (IM), maximum likelihood (ML) detection, reconfigurable intelligent surface (RIS), space shift keying (SSK).**

I. Introduction

SIXTH-GENERATION (6G) wireless networks, as well as the new technological trends they will introduce, are predicted to be accompanied by much more challenging engineering problems than their state-of-the-art counterparts. For instance, 6G wireless communication is anticipated to require very high spectral and energy efficiency in addition to ultra-high throughput per user, since over a hundred billion devices will have to be connected to highly data-intensive applications [1]. Considering also the jump to extremely high frequency bands, the transition to 6G networks will inevitably necessitate novel communication paradigms, especially in the physical layer.

One such paradigm is reconfigurable intelligent surface (RIS)-based transmission, which is attracting considerable interest in the literature currently. An RIS is mostly designed as a two-dimensional (2D) array of low-cost reflective units, which intentionally manipulate the characteristics of electromagnetic waves in propagation environments. This is done through a software and with the aim of enhancing the quality of service and/or expanding the network coverage. Each reflecting element can independently adjust the phase shift of the incoming signal, and as a result, the implicit randomness of the propagation environment can be utilized to create more efficient wireless channels through soft-controlled intelligent reflection.

Unlike traditional reflect-/transmit-array antennas, an RIS enables the dynamic shaping of the incident waves without the need for a separate energy source dedicated to radio frequency (RF) processing. As a passive reflecting apparatus, it also differs from the traditional relays that actively retransmit received signals. All the mentioned advantages make RIS popular as not only one of the key enablers of 6G technology but also as a promising solution to the energy consumption and hardware cost problems that are ever-present in the evolution of wireless networks. However, whether or not conventional communication systems can be upgraded to RIS-assisted forms involving passive elements has not yet been clarified.

The emerging concept of index modulation (IM) [2], which uses the indices of the available transmit entities to convey additional data bits, is worthy of discussion in this context, mainly due to its advantages in spectral and energy efficiency as well as in hardware simplicity. For instance, spatial modulation (SM) as an IM-based method, utilizes the index of transmitter (Tx) antennas to convey extra information. In [3], IM was integrated into the realm of RIS-assisted communications using three RIS-based schemes built upon the SM technique and its simplified version, space shift keying (SSK). Among them was a scheme that uses an RIS as an access point while realizing SM/SSK at the receiver (Rx). This was investigated in terms of error probability, and it was shown that high data rates can be achieved by using RIS-SM/SSK at the cost of remarkably low error rates. An energy-efficient RIS-based SSK scheme was introduced in [4] not only to provide reliable transmission, but also to avoid synchronization

Manuscript received 22 April 2022; revised 5 July 2022; accepted 6 July 2022. Date of publication 13 July 2022; date of current version 16 September 2022. The associate editor coordinating the review of this article and approving it for publication was Y. Liu. *(Corresponding author: Ayse E. Canbilen.)*

Ayse E. Canbilen is with the Electrical and Electronics Engineering Department, Konya Technical University, Selcuklu, 42250 Konya, Turkey (e-mail: aecanbilen@ktun.edu.tr).

Ertugrul Basar is with the Communications Research and Innovation Laboratory (CoreLab) and the Department of Electrical and Electronics Engineering, Koç University, Sariyer, 34450 Istanbul, Turkey (e-mail: ebasar@ku.edu.tr).

Salama S. Ikki is with the Department of Electrical Engineering, Lakehead University, Thunder Bay, ON P7B 5E1, Canada (e-mail: sikki@lakeheadu.ca).

Color versions of one or more figures in this article are available at https://doi.org/10.1109/TCOMM.2022.3190383.

Digital Object Identifier 10.1109/TCOMM.2022.3190383

and interference problems, and this was done by exploiting the SSK at the transmitter (Tx) side.

Motivated by these promising results, researchers kept designing novel RIS-SM/SSK schemes. For instance, RIS-aided receive quadrature reflecting modulation (RIS-RQRM), which outperformed earlier schemes, was designed by partitioning the RIS into two halves, each of which forms a beam to a specific Rx antenna according to the information bits [5]. However, reflection modulation schemes have the main drawback of underused RIS potential, and they can give rise to difficult optimization problems [6]. Another RIS-SSK scheme that grants knowledge of the active antenna index at the RIS and achieves passive beamforming by optimizing the reflection angles, was proposed in [7] alongside a scheme where RIS conveys its own Alamouti-coded data and reflects SSK signals to the Rx side. More recently, an RIS-assisted communication framework that adopts an ambient backscattering technique, along with advanced forms of SM, was presented in [8]. Additionally, RIS-assisted uplink communications using SM are investigated in [9].

As a matter of fact, physical realizations of RF transceivers suffer from the adverse effects of inherent hardware impairment (HWI), such as carrier-frequency and sampling-rate offset, quantization error, phase noise, amplifier non-linearity, and I/Q imbalance. Although some of these imperfections can be partially canceled out using calibration, pre-distortion or compensation techniques, an important amount of distortion is unavoidable in practical scenarios due to the imperfect estimation of time-variant hardware characteristics and the random noise [10], [11]. Therefore, the effects of HWI, the principal of which is major performance degradation, make up an important area to probe when evaluating the overall system performance [11].

Since there are also many previous works proving the undeniable destructive effects of the HWI on both SM-based [12]–[15] and RIS-aided [11], [16]–[20] transmission schemes, investigating the behavior of the RIS-assisted SM/SSK schemes against these imperfections is crucial. With this in mind, the performance of a blind RIS-SSK system was analyzed under the effect of HWI in [21]. However, that study does not provide much insight into the practical implementations of RIS, since a blind RIS, without a dynamic phase-adjustment, cannot really be used in a communication system. The study in [22] assumes an intelligent beamforming scenario, and demonstrated that the performance of the traditional SM with I/Q imbalance can be remarkably improved by the deployment of an RIS between the base station and the user.

The first RIS-SSK/SM schemes were introduced only about two years ago, and considering that this field is still in its infancy, further investigations are required to gain a clear understanding about their full potential wireless communication networks. As such, the intelligent RIS-SSK system proposed in [4] is discussed as a reference scheme by offering a more realistic Rx design in this study. However, it is observed that cancelling all the channel phases in this reference scheme through the RIS reduces the differences between the channels, which limits the performance of the SSK since it inherently needs a rich scattering environment.

Considering the abovementioned points, the main contributions of this work can be summarized as follows:

1) The performance restriction of the intelligent RIS-SSK scheme in [4] is resolved by two novel schemes, namely power sensing and partitioned RIS-SSK, both of which are proposed in this study.
2) The superiority of the power sensing and partitioned RIS-SSK schemes is proved by presenting their error performance analysis results, which are obtained under the assumption of perfect transceiver, and validated by computer simulations.
3) In order to have more realistic results, the ABER performances of the proposed schemes are also investigated in the case of hardware-impaired transceivers.
4) A computational complexity analysis is provided to enrich the discussion.
5) The effects of phase estimation errors at the RIS and path loss are investigated by computer simulations.

Organization: The system models of the proposed RIS-SSK schemes are given in Section II, while their error performance analyses are presented in Section III. The computational complexity is analyzed in Section IV. Then, extensive computer simulation results are presented in Section V, and finally, the study is concluded in Section VI.

Notations: The element of a matrix $\boldsymbol{A}$ in the ith row and jth column is specified by A_{ij}. The conjugate of a complex value z is denoted by z^* while its real and imaginary parts are shown by $\Re\{z\}$ and $\Im\{z\}$, respectively. The statistical expectation is represented by $\mathbb{E}\{\cdot\}$, and $\mathcal{CN}(\mu, \sigma^2)$ is used for a complex Gaussian random variable (RV) with mean μ and variance σ^2. $Pr\{\cdot\}$ stands for the probability of an event, while $Q(x) = \frac{1}{2\pi}\int_x^\infty \exp(\frac{-u^2}{2})du$ denotes the Q-function.

II. System Model

In this section, we present the system models for the proposed RIS-SSK schemes considering both ideal and non-ideal transceivers. We also discuss the idea of optimal reflection phase adjustment, which helps achieve the best error performance. We construct the proposed schemes by building on the intelligent RIS-SSK concept introduced in [4], where the RIS is equipped with N low-cost passive reconfigurable meta-elements and exploited as a reflector in a dual-hop communication system between N_t Tx antennas and one Rx antenna.[1] In this manner, we assume that SSK is applied by mapping the incoming bits to the index of a specific Tx antenna, which is activated to enable the transmission of an unmodulated carrier signal to the Rx through the RIS. For all scenarios, the Tx is assumed to be communicating with the Rx only through the RIS, due to physical obstacles.[2]

[1]Note that a multi-antenna Rx would not be a practical scenario for the proposed designs discussing optimal phase adjustment, since the reflector elements can be set at just one specific phase for each reflection. However, sub-optimal solutions can be utilized to realize this scenario, such as the cosine similarity theorem-based algorithm proposed in [23].

[2]Even if the Tx-Rx channel is not strictly null due to environment scattering, the direct path is domainated by the RIS links [4], and thus, does not have a major effect on the performance of the proposed systems for large N.

Moreover, the reflection phases are adjusted using a communication software so as to maximize the signal-to-noise ratio (SNR) at the Rx side. Unlike the RIS-SSK design in [4], the Rx is assumed to be unaware of the selected reflection phase in the first model, which is more practical, and this model is treated as a reference scheme. In line with this assumption, two novel RIS-SSK transceiver designs are presented with the principal aim of obtaining information on the activated Tx antenna during phase adjustment at the RIS.

The wireless fading channel between the tth Tx antenna of the base station and the ith reflecting element of the RIS is defined by $h_{t,i} = \alpha_{t,i}e^{-j\theta_{t,i}}$, while the channel between the ith RIS reflector and the Rx antenna is denoted by $g_i = \beta_i e^{-j\psi_i}$, for $t \in \{1, \ldots, N_t\}$ and $i = 1, \ldots, N$. Both of the channels are assumed to be following $\mathcal{CN}(0,1)$ distribution.[3] Additionally, in all the proposed models, the RIS has knowledge of the channel phases, i.e., $\theta_{t,i}$ and ψ_i, and the Rx has perfect channel state information, which is a common assumption of the optimal system behavior [3].

Although each type of HWI can be specified independently, the combined influence is modeled by the generalized impairment model given in [25], [26], and thus, all the noise is denoted by a single equivalent noise term. Accordingly, the distortion noises arising from the HWI effects in the Tx and Rx are represented by the parameters of η_{tx} and η_{rx}, which can be interpreted as the error vector magnitudes,[4] respectively.

A. Reference Intelligent RIS-SSK Scheme

1) Perfect Transceiver Case: The reference scheme has a system model that operates similar to that of the intelligent RIS-SSK system given in [4], save for the detector design, which is illustrated in Fig. 1. In this scenario, the received baseband signal at the Rx antenna can be written as:

$$y_{rp} = \sqrt{E}\left(\sum_{i=1}^{N} h_{t,i}e^{j\phi_{t,i}}g_i\right) + n, \tag{1}$$

where E is the transmitted signal energy, n is a zero-mean additive white Gaussian noise (AWGN) term with variance N_0. $\phi_{t,i}$ is the adjusted phase for the ith reflector of the RIS, determined by a communication software based on the activated Tx antenna t. Since the reflection phases are controlled by maximizing the instantaneous SNR value at the Rx side, it can be easily interpreted from [4] that $\phi_{t,i}$ should be adjusted as a phase value eliminating any channel phases, i.e., ensuring that $\phi_{t,i} = \theta_{t,i} + \psi_i$.

The fact remains that the activation of Tx antennas carries information in SSK, which implies that the update rate of the antenna activation is on the order of symbol rate, and thus, the RIS also needs to acquire this information at least at the same rate. A possible solution to this challenge is equipping the RIS with a cognitive device that has machine-learning ability. This would enable the RIS to continually observe the communication environment, make decisions and learn autonomously from past experiences [27].

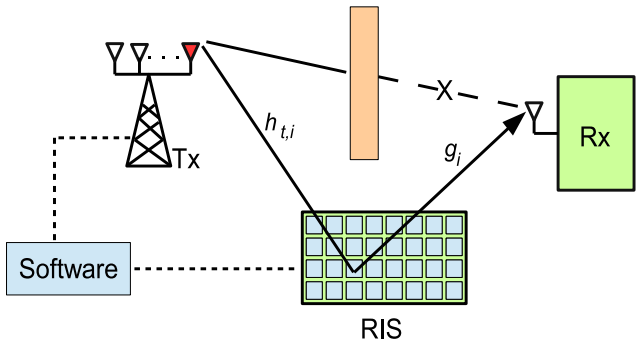

Fig. 1. Intelligent RIS-SSK scheme.

Considering the aforementioned points, a maximum likelihood (ML) detector, which determines the index of the activated Tx antenna, is designed for the reference intelligent RIS-SSK scheme as:

$$\hat{t} = \arg\min_{t} \left\{ \left| y_{rp} - \sqrt{E}\left(\sum_{i=1}^{N} \alpha_{t,i}\beta_i\right)\right|^2 \right\}. \tag{2}$$

2) Non-Ideal Transceiver Case: Considering the distortion noises at the Tx and Rx sides, which independently characterize the residual HWI effect, the received signal expression of the reference intelligent RIS-SSK can be written as follows:

$$\begin{aligned} y_{rn} &= \left(\sqrt{E} + \eta_{tx}\right)\left(\sum_{i=1}^{N} h_{t,i}e^{j\phi_{t,i}}g_i\right) + \eta_{rx} + n, \\ &= \underbrace{\sqrt{E}\left(\sum_{i=1}^{N} h_{t,i}e^{j\phi_{t,i}}g_i\right)}_{\text{Desired signal}} + \underbrace{\eta_{tx}\left(\sum_{i=1}^{N} h_{t,i}e^{j\phi_{t,i}}g_i\right) + \eta_{rx} + n}_{\text{Noise}}, \end{aligned} \tag{3}$$

where η_{tx} and η_{rx} follow the respective distributions of $\mathcal{CN}(0, \kappa_{tx}^2 E)$ and $\mathcal{CN}(0, \kappa_{rx}^2(E|\sum_{i=1}^{N} h_{t,i}e^{j\phi_{t,i}}g_i|^2))$ [21]. According to (3), the instantaneous signal-to-total noise ratio, which can also be considered the signal-to-noise-and-distortion ratio (SDNR), is given by:

$$\text{SDNR}_{rn} = \frac{E\left|\sum_{i=1}^{N} h_{t,i}e^{j\phi_{t,i}}g_i\right|^2}{E\left(\kappa_{tx}^2 + \kappa_{rx}^2\right)\left|\sum_{i=1}^{N} h_{t,i}e^{j\phi_{t,i}}g_i\right|^2 + N_0}. \tag{4}$$

Noting that the values chosen for parameters κ_{tx} and κ_{rx} are usually very small [21], [25], $\kappa_{tx}, \kappa_{rx} \ll 1$, increasing the value of the term $|\sum_{i=1}^{N} h_{t,i}e^{j\phi_{t,i}}g_i|^2$ in (4) will cause an increment in the numerator more than in the denominator. Hence, by adjusting the reflector phases to maximize this term, the SDNR will in turn be maximized: $\phi_{t,i} = \theta_{t,i} + \psi_i$ [4]. Correspondingly, (3) can be rewritten as:

$$y_{rn} = \sqrt{E}\left(\sum_{i=1}^{N} \alpha_{t,i}\beta_i\right) + w, \tag{5}$$

[3]Rayleigh fading model is chosen for this preliminary study to provide the basis for further theoretical research in RIS-based multiple antenna systems, since it leads to neat and understandable closed-form expressions [24].

[4]Error vector magnitude is the average distortion magnitude to average signal magnitude ratio [21].

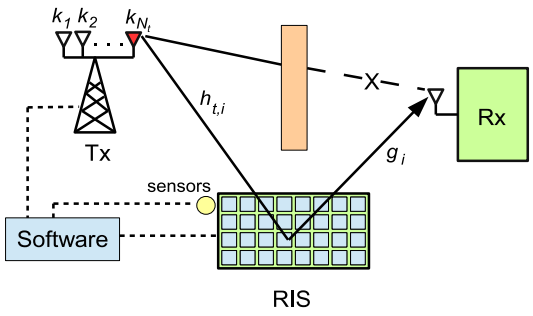

Fig. 2. Power-sensing RIS-SSK scheme.

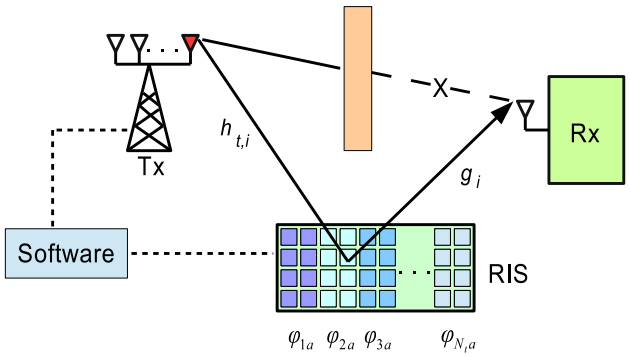

Fig. 3. Partitioned RIS-SSK scheme.

where $w = \eta_{tx}\big(\sum_{i=1}^{N}\alpha_{t,i}\beta_i\big) + \eta_{rx} + n$ has zero-mean with the following variance value:

$$\sigma_w^2 = \kappa^2 E\left|\sum_{i=1}^{N}\alpha_{t,i}\beta_i\right|^2 + N_0, \tag{6}$$

where $\kappa^2 = \kappa_{tx}^2 + \kappa_{rx}^2$ represents the aggregate level of HWI. Then, an optimal ML detector is designed for the reference RIS-SSK scheme under the assumption of a non-ideal transceiver as follows:

$$\hat{t} = \arg\min_t \left\{\left|y_{rn} - \sqrt{E}\Big(\sum_{i=1}^{N}\alpha_{t,i}\beta_i\Big)\right|^2\right\}. \tag{7}$$

B. Power Sensing RIS-SSK Scheme

1) Perfect Transceiver Case: The system model of the power sensing RIS-SSK scheme, which obtains knowledge of the active Tx antenna index from the embedded low-cost sensors [27] throughout the RIS, is given in Fig. 2. In this scheme, each Tx antenna conveys the unmodulated carrier signal with a different level of power assigned to that specific antenna on the condition of a fixed average power.

The sensors, possibly powered by energy-harvesting modules, are in charge of detecting the power level of the incoming signals, and thus acquiring the activation status of the Tx antennas. Thus, the reflection phases can be adjusted for that transmission instant by receiving, through the communication software, updates from the sensors. Accordingly, the received signal at the Rx through the RIS, can be written as:

$$y_{pp} = \sqrt{Ek_t}\left(\sum_{i=1}^{N} h_{t,i}e^{j\phi_{t,i}}g_i\right) + n, \tag{8}$$

where $k_t = (2t-1)/N_t$ is the power constant for the tth Tx antenna, and $\phi_{t,i}$ is specified similar to what was done in Section II-A-1. Now, an optimal ML detector, which identifies the index of the activated Tx antenna can be defined as follows:

$$\hat{t} = \arg\min_t \left\{\left|y_{pp} - \sqrt{Ek_t}\left(\sum_{i=1}^{N}\alpha_{t,i}\beta_i\right)\right|^2\right\}. \tag{9}$$

2) Non-Ideal Transceiver Case: Considering the distortion noises stemming from the HWIs, the received signal for the power sensing RIS-SSK can be written as:

$$y_{pn} = \left(\sqrt{Ek_t} + \eta_{tx}\right)\left(\sum_{i=1}^{N} h_{t,i}e^{j\phi_{t,i}}g_i\right) + \eta_{rx} + n$$

$$= \underbrace{\sqrt{Ek_t}\Big(\sum_{i=1}^{N} h_{t,i}e^{j\phi_{t,i}}g_i\Big)}_{\text{Desired signal}} + \underbrace{\eta_{tx}\Big(\sum_{i=1}^{N} h_{t,i}e^{j\phi_{t,i}}g_i\Big) + \eta_{rx} + n}_{\text{Noise}}, \tag{10}$$

where η_{tx} and η_{rx} follow the same distributions as in (3) since the average power is maintained as E here. Clearly, the instantaneous SDNR value can be obtained by writing Ek_t instead of E in the numerator of (4) for this scenario, and the value of the SDNR can be maximized by following the same procedure. Therefore, the received signal at the Rx can be given by:

$$y_{pn} = \sqrt{Ek_t}\Big(\sum_{i=1}^{N}\alpha_{t,i}\beta_i\Big) + w, \tag{11}$$

where w is as defined in (5). Hence for the power sensing RIS-SSK scheme with HWI, an optimal ML detector can be designed by utilizing (11) as follows:

$$\hat{t} = \arg\min_t \left\{\left|y_{pn} - \sqrt{Ek_t}\left(\sum_{i=1}^{N}\alpha_{t,i}\beta_i\right)\right|^2\right\}. \tag{12}$$

C. Partitioned RIS-SSK Scheme

1) Perfect Transceiver Case: In the partitioned RIS-SSK scheme shown in Fig. 3, the elements of the RIS are partitioned into N_t groups, each having N/N_t number of elements, and all reflecting the signals that strike them at a certain predetermined angle, $\phi_{t,a}$ for $t \in \{1,\ldots,N_t\}$ and $a = 1,\ldots,(N/N_t)$. Here, the reflection phase of the tth reflector group is adjusted so as to eliminate the phases of the channels utilized to convey the signal received from the tth Tx antenna to the Rx through that group, i.e., $\phi_{t,a} = \theta_{t,a} + \psi_a$. For instance, assuming that the first Tx antenna is utilized for a transmission instant, and keeping in mind that only one antenna will be activated for transmission, only the phases of the channels created by the first reflector group are canceled out.

Hence, this scheme offers more diversity for the transmission channel since the phases are not entirely canceled out at the RIS. Because the performance of SSK highly depends on the distinctness of the channel signatures associated with different active antennas, this scheme is expected to enhance the overall system performance seen in the reference RIS-SSK scheme detailed in Section II-A. Hence, cancelling the channel phases at only N/N_t elements can turn into an advantage despite losing array gain.

The received signal for the partitioned RIS-SSK scheme, under the assumption of perfect hardware, can be written by considering the aforementioned points as follows:

$$y_p = \sqrt{E}\left(\sum_{k=1}^{N_t}\left(\sum_{i=\frac{(k-1)N}{N_t}+1}^{k\frac{N}{N_t}} h_{t,i}e^{j\phi_{k,i}}g_i\right)\right) + n, \quad (13)$$

where $\phi_{k,i} = \theta_{k,i}+\psi_i$. Following that, an optimal ML detector can be designed as:

$$\hat{t} = \arg\min_{t}\left\{\left|y_p - \sqrt{E}\sum_{k=1}^{N_t}\left(\sum_{i=\frac{(k-1)N}{N_t}+1}^{k\frac{N}{N_t}} h_{t,i}e^{j\phi_{k,i}}g_i\right)\right|^2\right\}. \quad (14)$$

2) Non-Ideal Transceiver Case: Considering the distortion noises due to the residual HWI effects, the received signal expression of the partitioned RIS-SSK can be expressed by:

$$y_n = \underbrace{\sqrt{E}\left(\sum_{k=1}^{N_t}\left(\sum_{i=\frac{(k-1)N}{N_t}+1}^{k\frac{N}{N_t}} h_{t,i}e^{j\phi_{k,i}}g_i\right)\right)}_{\text{Desired Signal}} + \underbrace{\eta_{tx}\left(\sum_{k=1}^{N_t}\left(\sum_{i=\frac{(k-1)N}{N_t}+1}^{k\frac{N}{N_t}} h_{t,i}e^{j\phi_{k,i}}g_i\right)\right) + \eta_{rx} + n}_{\text{Noise}}, \quad (15)$$

where η_{tx} follows the same distribution as in (3), while η_{rx} follows a zero-mean Gauss distribution with the following variance value:

$$\sigma^2_{\eta_{rx}} = \kappa^2_{rx}E\left|\left(\sum_{k=1}^{N_t}\left(\sum_{i=\frac{(k-1)N}{N_t}+1}^{k\frac{N}{N_t}} h_{t,i}e^{j\phi_{k,i}}g_i\right)\right)\right|^2. \quad (16)$$

Representing the noise part in (15) with Δ, the received signal at the Rx antenna can be rewritten as follows:

$$y_n = \sqrt{E}\left(\sum_{k=1}^{N_t}\left(\sum_{i=\frac{(k-1)N}{N_t}+1}^{k\frac{N}{N_t}} h_{t,i}e^{j\phi_{k,i}}g_i\right)\right) + \Delta, \quad (17)$$

where Δ follows $\mathcal{CN}(0,\sigma^2_\Delta)$ with:

$$\sigma^2_\Delta = \kappa^2 E\left|\left(\sum_{k=1}^{N_t}\left(\sum_{i=\frac{(k-1)N}{N_t}+1}^{k\frac{N}{N_t}} h_{t,i}e^{j\phi_{k,i}}g_i\right)\right)\right|^2 + N_0. \quad (18)$$

After that, an optimal ML detector can be designed by using (17) for the partitioned RIS-SSK under the assumption of a non-ideal transceiver as follows:

$$\hat{t} = \arg\min_{t}\left\{\left|y_n - \sqrt{E}\sum_{k=1}^{N_t}\left(\sum_{i=\frac{(k-1)N}{N_t}+1}^{k\frac{N}{N_t}} h_{t,i}e^{j\phi_{k,i}}g_i\right)\right|^2\right\}. \quad (19)$$

III. Performance Analysis

In this section, we present error performance analyses for the proposed RIS-SSK schemes considering both the ideal and non-ideal transceiver cases. In particular, we calculate the average pairwise error probability (APEP) for each scheme by using optimal ML detectors given in the previous sections. We then propose a union bound technique to calculate the average bit error rate (ABER).

A. Performance of the Reference Intelligent RIS-SSK Scheme

1) Perfect Transceiver Case: Assuming the activation of Tx antenna t for the transmission of an unmodulated carrier signal to the RIS to be reflected to Rx, and assuming its erroneous detection to be $\hat{t}$, the conditional pairwise error probability (CPEP) expression can be obtained for the reference intelligent RIS-SSK scheme by using the ML detection rule given in (2) as follows:

$$P_e = Pr\left\{|y_{rp} - \sqrt{E}G_t|^2 > |y_{rp} - \sqrt{E}G_{\hat{t}}|^2\right\}, \quad (20)$$

where $G_t = \sum_{i=1}^{N}\alpha_{t,i}\beta_i$, $G_{\hat{t}} = \sum_{i=1}^{N}\alpha_{\hat{t},i}\beta_i$. After some mathematical operations, (20) can be rewritten as $P_e = Pr\{\Upsilon_p > 0\}$, where $\Upsilon_p = -E|G_t - G_{\hat{t}}|^2 - 2\Re\{\sqrt{E}(G_t - G_{\hat{t}})n^*\}$ is a complex Gaussian RV following $\mathcal{CN}(\mu_{\Upsilon_p}, \sigma^2_{\Upsilon_p})$ with $\mu_{\Upsilon_p} = -E|G_t - G_{\hat{t}}|^2$ and $\sigma^2_{\Upsilon_p} = 2EN_0|G_t - G_{\hat{t}}|^2$. After that, the CPEP can also be written as follows:

$$P_e = Q\left(\sqrt{\frac{E|\sum_{i=1}^{N}\beta_i(\alpha_{t,i} - \alpha_{\hat{t},i})|^2}{2N_0}}\right). \quad (21)$$

Then, the APEP value can be derived by averaging (21), yielding:

$$\overline{P}_e = \int_0^\infty Q\left(\sqrt{\frac{E\lambda}{2N_0}}\right) f_\lambda(\lambda)d\lambda, \quad (22)$$

where $\lambda = |B|^2 = |\sum_{i=1}^{N}\beta_i(\alpha_{t,i} - \alpha_{\hat{t},i})|^2$ and $f_\lambda(\lambda)$ is the probability density function (pdf) of λ, which follows a central chi-square distribution with one degree of freedom. Besides, noting that B is a zero-mean Gaussian RV with a variance value of σ^2_B, and considering the Central Limit Theorem (CLT) for a sufficiently large number of reflecting elements, $N \gg 1$, and realizing that $(\alpha_{t,i} - \alpha_{\hat{t},i})$ and β_i are independent, σ^2_B is calculated as $\sigma^2_B = N(2 - \pi/2)$.

For the sake of simplicity, the APEP is computed by utilizing the moment-generating function (MGF) of λ, which can be given by $M_\lambda(t) = (1 - 2\sigma^2_B t)^{-1/2}$, as an alternative to (22). This way, the APEP is obtained as follows [22]:

$$\begin{aligned}\overline{P}_e &= \frac{1}{\pi}\int_0^{\frac{\pi}{2}} M_\lambda\left(\frac{-E}{4N_0\sin^2\eta}\right)d\eta \\ &= \frac{1}{\pi}\int_0^{\frac{\pi}{2}}\left(\frac{1}{\sqrt{1 + (2 - \frac{\pi}{2})\frac{NE}{2N_0\sin^2\eta}}}\right)d\eta. \end{aligned} \quad (23)$$

2) Non-Ideal Transceiver Case: In this case, the system equipment is considered non-ideal at both the Tx and Rx sides. Assume that the signal is conveyed to the RIS with the tth Tx antenna; however, it has been detected erroneously as $\hat{t}$ at the Rx side, so the CPEP is calculated by using (7) as follows:

$$\begin{aligned} P_e &= Pr\left\{|y_{rn} - \sqrt{E}G_t|^2 > |y_{rn} - \sqrt{E}G_{\hat{t}}|^2\right\} \\ &= Pr\left\{-E|G_t - G_{\hat{t}}|^2 - 2\Re\{\sqrt{E}(G_t - G_{\hat{t}})w^*\} > 0\right\} \\ &= Pr\{\Upsilon_n > 0\}, \end{aligned} \tag{24}$$

where $\Upsilon_n \sim \mathcal{CN}(\mu_{\Upsilon_n}, \sigma^2_{\Upsilon_n})$ with $\mu_{\Upsilon_n} = -E|G_t - G_{\hat{t}}|^2$ and $\sigma^2_{\Upsilon_n} = 2E(\kappa^2 E|\sum_{i=1}^{N} \alpha_{t,i}\beta_i|^2 + N_0)|G_t - G_{\hat{t}}|^2$, while G_t and $G_{\hat{t}}$ are as defined in (20). Then, the CPEP is given by:

$$P_e = Q\left(\sqrt{\frac{E\lambda}{2(\kappa^2 E|\sum_{i=1}^{N} \alpha_{t,i}\beta_i|^2 + N_0)}}\right), \tag{25}$$

where λ is the same as defined in (22). By CLT, it can be said that $\sum_{i=1}^{N} \alpha_{t,i}\beta_i$ follows a zero-mean Gaussian distribution for a large number of reflectors. Then, an approximation to (25) can be obtained by replacing the term $|\sum_{i=1}^{N} \alpha_{t,i}\beta_i|^2$ with its expected value, i.e., $\mathbb{E}\{|\sum_{i=1}^{N} \alpha_{t,i}\beta_i|^2\} = N(\frac{16-\pi^2}{16})$ [12], [18]. As a result, utilizing also the MGF of λ by following the same procedure in the previous section, the APEP can be rewritten as follows:

$$\overline{P}_e \approx \frac{1}{\pi}\int_0^{\frac{\pi}{2}} \frac{1}{\sqrt{1 + \frac{NE(2-\pi/2)}{2\left(\kappa^2 EN(\frac{16-\pi^2}{16}) + N_0\right)\sin^2\eta}}} d\eta. \tag{26}$$

It is worth noting here that the APEP value is dependent on neither N nor E in the high SNR region, since (26) turns into the following statement under the assumption of $E \gg 1$:

$$\overline{P}_e \approx \frac{1}{\pi}\int_0^{\frac{\pi}{2}} \frac{1}{\sqrt{1 + \frac{4}{\kappa^2(4+\pi)\sin^2\eta}}} d\eta, \tag{27}$$

which leads to the following remark.

Remark 1: The destructive effect of HWI limits the overall system performance of the reference intelligent RIS-SSK scheme even if the number of reflecting elements, N, grows infinitely large in the high SNR region. Besides that, non-ideal transceivers will clearly cause an error floor, since increasing E would not help enhance the quality of the service for this scheme.

B. Performance of the Power Sensing RIS-SSK Scheme

1) Perfect Transceiver Case: Assume that the unmodulated carrier signal generated by source is conveyed to the RIS with Tx antenna t; however, it has been detected erroneously that the signal was transmitted through the Tx antenna $\hat{t}$ at the Rx side, so the CPEP is calculated by using (9) as follows:

$$\begin{aligned} P_e &= Pr\{|y_{pp} - \sqrt{Ek_t}G_t|^2 > |y_{pp} - \sqrt{Ek_{\hat{t}}}G_{\hat{t}}|^2\} \\ &= Pr\big\{ -E|\sqrt{k_t}G_t - \sqrt{k_{\hat{t}}}G_{\hat{t}}|^2 \\ &\quad - 2\Re\{\sqrt{E}(\sqrt{k_t}G_t - \sqrt{k_{\hat{t}}}G_{\hat{t}})n^*\} > 0\big\} \\ &= Pr\{\Theta_p > 0\}, \end{aligned} \tag{28}$$

where G_t and $G_{\hat{t}}$ are as defined in (20), $k_{\hat{t}} = (2\hat{t} - 1)/N_t$, and Θ_p is a complex Gaussian RV with a mean value of $\mu_{\Theta_p} = -E|\sqrt{k_t}G_t - \sqrt{k_{\hat{t}}}G_{\hat{t}}|^2$ and a variance of $\sigma^2_{\Theta_p} = 2EN_0|\sqrt{k_t}G_t - \sqrt{k_{\hat{t}}}G_{\hat{t}}|^2$. Following that, the CPEP can be written by:

$$P_e = Q\left(\sqrt{\frac{E\left|\sum_{i=1}^{N} \beta_i(\sqrt{k_t}\alpha_{t,i} - \sqrt{k_{\hat{t}}}\alpha_{\hat{t},i})\right|^2}{2N_0}}\right). \tag{29}$$

Here, defining $\Lambda = |\delta|^2 = \left|\sum_{i=1}^{N} \beta_i(\sqrt{k_t}\alpha_{t,i} - \sqrt{k_{\hat{t}}}\alpha_{\hat{t},i})\right|^2$, it can be stated that $\delta \sim \mathcal{CN}(\mu_\delta, \sigma^2_\delta)$ according to CLT, and thus, Λ follows the non-central chi-square distribution with one degree of freedom. Then, realizing that $(\sqrt{k_t}\alpha_{t,i} - \sqrt{k_{\hat{t}}}\alpha_{\hat{t},i})$ and β_i are independent, μ_δ and σ^2_δ can be given as:

$$\mu_\delta = N\pi\left(\frac{\sqrt{k_t} - \sqrt{k_{\hat{t}}}}{4}\right), \tag{30}$$

$$\sigma^2_\delta = N\left\{\left(1 - \left(\frac{\pi}{4}\right)^2\right)(k_t + k_{\hat{t}}) - \frac{\pi(4-\pi)}{8}\sqrt{k_t k_{\hat{t}}}\right\}. \tag{31}$$

Utilizing the MGF of Λ, which can be given by $M_\Lambda(t) = (1-2\sigma^2_\delta t)^{-1/2} \times \exp(\mu^2_\delta t/(1-2\sigma^2_\delta t))$, the APEP of the power sensing RIS-SSK scheme can be calculated by substituting (31) into the following statement:

$$\begin{aligned} \overline{P}_e = \frac{1}{\pi}\int_0^{\frac{\pi}{2}} &\frac{1}{\sqrt{1 + 2\sigma^2_\delta \times \frac{E}{4N_0\sin^2\eta}}} \\ &\times \exp\left(\frac{N^2\pi^2\left(\frac{\sqrt{k_t}-\sqrt{k_{\hat{t}}}}{4}\right)^2 \times \frac{-E}{4N_0\sin^2\eta}}{1 - 2\sigma^2_\delta \times \frac{E}{4N_0\sin^2\eta}}\right) d\eta. \end{aligned} \tag{32}$$

2) Non-Ideal Transceiver Case: If the transceiver of the power sensing RIS-SSK scheme is non-ideal at both the Tx and Rx sides, and thus, the system is exposed to the destructive effect of HWI, then the CPEP can be calculated by using the ML rule provided in (12) for the wrong detection of Tx antenna t as follows:

$$\begin{aligned} P_e &= Pr\{\left|y_{pn} - \sqrt{Ek_t}G_t\right|^2 > \left|y_{pn} - \sqrt{Ek_{\hat{t}}}G_{\hat{t}}\right|^2\} \\ &= Pr\{-E|\sqrt{k_t}G_t - \sqrt{k_{\hat{t}}}G_{\hat{t}}|^2 \\ &\quad - 2\Re\{\sqrt{E}(\sqrt{k_t}G_t - \sqrt{k_{\hat{t}}}G_{\hat{t}})w^*\} > 0\} \\ &= Pr\{\Theta_n > 0\}, \end{aligned} \tag{33}$$

where Θ_n is a Gaussian RV that follows $\mathcal{CN}(\mu_{\Theta_n}, \sigma^2_{\Theta_n})$ for $\sigma^2_{\Theta_n} = 2E(\kappa^2 E\left|\sum_{i=1}^{N} \alpha_{t,i}\beta_i\right|^2 + N_0)|\sqrt{k_t}G_t - \sqrt{k_{\hat{t}}}G_{\hat{t}}|^2$ and $\mu_{\Theta_n} = -E|\sqrt{k_t}G_t - \sqrt{k_{\hat{t}}}G_{\hat{t}}|^2$. Now, utilizing μ_{Θ_n}, $\sigma^2_{\Theta_n}$ and the Q-function, the CPEP expression of the power sensing RIS-SSK in the presence of HWI is obtained as:

$$P_e = Q\left(\sqrt{\frac{E\Lambda}{2(\kappa^2 E\left|\sum_{i=1}^{N} \alpha_{t,i}\beta_i\right|^2 + N_0)}}\right), \tag{34}$$

where $\Lambda = |\delta|^2$ is the same as the one defined in (29). Realizing that $\varsigma = \sum_{i=1}^{N} \alpha_{t,i}\beta_i$ follows a zero-mean Gaussian distribution for a large number of reflectors according to CLT, the term $|\sum_{i=1}^{N} \alpha_{t,i}\beta_i|^2$ in the denominator of (34) can be replaced by its expected value, which is equal to the variance of ς, i.e., $\sigma^2_\varsigma = N(\frac{16-\pi^2}{16})$. Then, using the MGF of Λ and

substituting σ_ς^2 in the following statement, an approximated APEP value can be achieved:

$$\overline{P}_e \approx \frac{1}{\pi}\int_0^{\frac{\pi}{2}} \frac{1}{\sqrt{1+2\sigma_\delta^2 \times \frac{E}{4(\kappa^2 E\sigma_\varsigma^2+N_0)\sin^2\eta}}} \times \exp\left(\frac{N^2\pi^2\left(\frac{\sqrt{k_t}-\sqrt{k_{\hat{t}}}}{4}\right)^2 \times \frac{-E}{4(\kappa^2 E\sigma_\varsigma^2+N_0)\sin^2\eta}}{1+2\sigma_\delta^2 \times \frac{E}{4(\kappa^2 E\sigma_\varsigma^2+N_0)\sin^2\eta}}\right) d\eta. \tag{35}$$

It should be noted here that the APEP value is not dependent on E in the high SNR region, i.e., $E \gg 1$, since (35) turns into the following statement under this condition:

$$\overline{P}_e = \frac{1}{\pi}\int_0^{\frac{\pi}{2}} \frac{1}{\sqrt{1+\left[\frac{(k_t+k_{\hat{t}})}{2} - \frac{\pi\sqrt{k_t k_{\hat{t}}}}{(4+\pi)}\right]\frac{1}{\kappa^2\sin^2\eta}}} \times \exp\left(\frac{-N\pi^2(\sqrt{k_t}-\sqrt{k_{\hat{t}}})^2}{(16-\pi^2)[4\kappa^2\sin^2\eta+\frac{k_t+k_{\hat{t}}}{2}]-(4\pi-\pi^2)\sqrt{k_t k_{\hat{t}}}}\right) d\eta, \tag{36}$$

which results in the following remark.

Remark 2: The use of non-ideal transceivers limit the overall system performance of the power sensing RIS-assisted SSK scheme for the high SNR region, and an error floor is expected to be observed. However, contrary to the reference intelligent RIS-SSK scheme, it is clear that increasing number of reflecting elements still improves the system performance, since increasing N leads to lower values of (36).

C. Performance of the Partitioned RIS-SSK Scheme

1) Perfect Transceiver Case: In that case, assuming that the signal is conveyed to the RIS with Tx antenna t, but it has been erroneously detected as $\hat{t}$; the CPEP expression can be written by using (14) as follows:

$$\begin{aligned} P_e = P\Bigg\{ \Bigg| y_p - \sqrt{E}\Bigg(& \sum_{i=\frac{(t-1)N}{N_t}+1}^{t\frac{N}{N_t}} \alpha_{t,i}\beta_i + \sum_{\substack{k=1\\k\neq t}}^{N_t} \sum_{i=\frac{(k-1)N}{N_t}+1}^{k\frac{N}{N_t}} \alpha_{t,i}\beta_i e^{j(\theta_{k,i}-\theta_{t,i})}\Bigg)\Bigg|^2 \\ > \Bigg| y_p - \sqrt{E}\Bigg(& \sum_{i=\frac{(\hat{t}-1)N}{N_t}+1}^{\hat{t}\frac{N}{N_t}} \alpha_{\hat{t},i}\beta_i + \sum_{\substack{k=1\\k\neq \hat{t}}}^{N_t} \sum_{i=\frac{(k-1)N}{N_t}+1}^{k\frac{N}{N_t}} \alpha_{\hat{t},i}\beta_i e^{j(\theta_{k,i}-\theta_{\hat{t},i})}\Bigg)\Bigg|^2\Bigg\}. \end{aligned} \tag{37}$$

After some tedious mathematical operations, and by defining $\zeta_i = \alpha_{t,i} - \alpha_{\hat{t},i}e^{j(\theta_{t,i}-\theta_{\hat{t},i})}$, $\xi_i = \alpha_{t,i}e^{j(\theta_{\hat{t},i}-\theta_{t,i})} - \alpha_{\hat{t},i}$ and $\Psi_i = \alpha_{t,i}e^{j(\theta_{k,i}-\theta_{t,i})} - \alpha_{\hat{t},i}e^{j(\theta_{k,i}-\theta_{\hat{t},i})}$, the CPEP can be rewritten as:

$$\begin{aligned} P_e = Pr\Bigg\{ -E\Bigg| & \Bigg(\sum_{i=\frac{(t-1)N}{N_t}+1}^{t\frac{N}{N_t}} \beta_i\zeta_i + \sum_{i=\frac{(\hat{t}-1)N}{N_t}+1}^{\hat{t}\frac{N}{N_t}} \beta_i\xi_i + \sum_{\substack{k=1\\k\neq t\\k\neq\hat{t}}}^{N_t} \sum_{i=\frac{(k-1)N}{N_t}+1}^{k\frac{N}{N_t}} \beta_i\Psi_i\Bigg)\Bigg|^2 \\ & - 2\Re\Bigg\{\sqrt{E}\Bigg(\sum_{i=\frac{(t-1)N}{N_t}+1}^{t\frac{N}{N_t}} \beta_i\zeta_i + \sum_{i=\frac{(\hat{t}-1)N}{N_t}+1}^{\hat{t}\frac{N}{N_t}} \beta_i\xi_i + \sum_{\substack{k=1\\k\neq t\\k\neq\hat{t}}}^{N_t} \sum_{i=\frac{(k-1)N}{N_t}+1}^{k\frac{N}{N_t}} \beta_i\Psi_i\Bigg) n^* > 0\Bigg\} \\ = Pr\{\Omega_p > 0\}, \end{aligned} \tag{38}$$

where Ω_p follows $\mathcal{CN}(\mu_{\Omega_p}, \sigma_{\Omega_p}^2)$ for $\sigma_{\Omega_p}^2 = 2EN_0|\gamma|^2$ and $\mu_{\Omega_p} = -E|\gamma|^2$, while

$$\gamma = \sum_{i=\frac{(t-1)N}{N_t}+1}^{t\frac{N}{N_t}} \beta_i\zeta_i + \sum_{i=\frac{(\hat{t}-1)N}{N_t}+1}^{\hat{t}\frac{N}{N_t}} \beta_i\xi_i + \sum_{\substack{k=1\\k\neq t\\k\neq\hat{t}}}^{N_t} \sum_{i=\frac{(k-1)N}{N_t}+1}^{k\frac{N}{N_t}} \beta_i\Psi_i. \tag{39}$$

Then, by utilizing Q-function, the CPEP is concluded as:

$$P_e = Q\left(\sqrt{\frac{E|\gamma|^2}{2N_0}}\right). \tag{40}$$

In (40), it can be easily written that $|\gamma|^2 = |\gamma^I|^2 + |\gamma^Q|^2$ while $\gamma^I \sim \mathcal{N}(\mu_{\gamma^I}, \sigma_{\gamma^I}^2)$ and $\gamma^Q \sim \mathcal{N}(\mu_{\gamma^Q}, \sigma_{\gamma^Q}^2)$ are the real and imaginary components of γ, which can be given as:

$$\begin{aligned} \gamma^I = & \sum_{i=\frac{(t-1)N}{N_t}+1}^{t\frac{N}{N_t}} \beta_i\left(\alpha_{t,i} - \Re\{\alpha_{\hat{t},i}e^{j(\theta_{t,i}-\theta_{\hat{t},i})}\}\right) \\ & + \sum_{i=\frac{(\hat{t}-1)N}{N_t}+1}^{\hat{t}\frac{N}{N_t}} \beta_i\left(\Re\{\alpha_{t,i}e^{j(\theta_{\hat{t},i}-\theta_{t,i})}\} - \alpha_{\hat{t},i}\right) \\ & + \sum_{\substack{k=1\\k\neq t\\k\neq\hat{t}}}^{N_t} \sum_{i=\frac{(k-1)N}{N_t}+1}^{k\frac{N}{N_t}} \beta_i \\ & \times \Re\{\alpha_{t,i}e^{j(\theta_{\hat{t},i}-\theta_{t,i})} - \alpha_{\hat{t},i}e^{j(\theta_{t,i}-\theta_{\hat{t},i})}\}, \end{aligned} \tag{41}$$

$$\begin{aligned} \gamma^Q = & \sum_{i=\frac{(\hat{t}-1)N}{N_t}+1}^{\hat{t}\frac{N}{N_t}} \beta_i\Im\{\alpha_{t,i}e^{j(\theta_{\hat{t},i}-\theta_{t,i})}\} \\ & - \sum_{i=\frac{(t-1)N}{N_t}+1}^{t\frac{N}{N_t}} \beta_i\Im\{\alpha_{\hat{t},i}e^{j(\theta_{t,i}-\theta_{\hat{t},i})}\} \end{aligned}$$

$$+\sum_{\substack{k=1\\k\neq t\\k\neq\hat{t}}}^{N_t}\sum_{i=\frac{(k-1)N}{N_t}+1}^{k\frac{N}{N_t}}\beta_i\Im\{\alpha_{t,i}e^{j(\theta_{\hat{t},i}-\theta_{t,i})}-\alpha_{\hat{t},i}e^{j(\theta_{t,i}-\theta_{\hat{t},i})}\}. \tag{42}$$

It is obvious from (41) and (42) that $\mu_{\gamma^I}=\mu_{\gamma^Q}=0$, while $\sigma^2_{\gamma^I}$ and $\sigma^2_{\gamma^Q}$ can be calculated as follows:

$$\sigma^2_{\gamma^I}=\frac{N}{N_t}\left(\frac{8-\pi^2}{8}+N_t\right),\quad \sigma^2_{\gamma^Q}=\frac{N}{N_t}(N_t-1). \tag{43}$$

Noting that $|\gamma|^2$ is a linear combination of two independent central chi-squared RVs with one degree of freedom, and utilizing the MGF of $|\gamma|^2$, which can be given by $M_{|\gamma|^2}(t)=[(1-2\sigma^2_{\gamma^I}t)\times(1-2\sigma^2_{\gamma^Q}t)]^{-1/2}$, the APEP is obtained as:

$$\overline{P}_e=\frac{1}{\pi}\int_0^{\frac{\pi}{2}}\frac{d\eta}{\sqrt{\left(1+\frac{NE(8-\pi^2+8N_t)}{16N_0N_t\sin^2\eta}\right)\left(1+\frac{NE(N_t-1)}{2N_0N_t\sin^2\eta}\right)}}. \tag{44}$$

2) Non-Ideal Transceiver Case: Considering the HWI effects at both the Tx and Rx, and assuming that the signal is transmitted to the RIS with the tth Tx antenna, the CPEP expression is obtained from (19). It can be easily achieved by writing y_n, which is defined in (15), instead of y_p in (37).

After some extensive mathematical operations, the CPEP can also be written as:

$$\begin{aligned}P_e=Pr\Bigg\{-E\Bigg|\Bigg(&\sum_{i=\frac{(t-1)N}{N_t}+1}^{t\frac{N}{N_t}}\beta_i\zeta_i+\sum_{i=\frac{(\hat{t}-1)N}{N_t}+1}^{\hat{t}\frac{N}{N_t}}\beta_i\xi_i\\&+\sum_{\substack{k=1\\k\neq t\\k\neq\hat{t}}}^{N_t}\sum_{i=\frac{(k-1)N}{N_t}+1}^{k\frac{N}{N_t}}\beta_i\Psi_i\Bigg)\Bigg|^2\\&-2\Re\Bigg\{\sqrt{E}\Bigg(\sum_{i=\frac{(t-1)N}{N_t}+1}^{t\frac{N}{N_t}}\beta_i\zeta_i+\sum_{i=\frac{(\hat{t}-1)N}{N_t}+1}^{\hat{t}\frac{N}{N_t}}\beta_i\xi_i\\&+\sum_{\substack{k=1\\k\neq t\\k\neq\hat{t}}}^{N_t}\sum_{i=\frac{(k-1)N}{N_t}+1}^{k\frac{N}{N_t}}\beta_i\Psi_i\Bigg)\Delta^*>0\Bigg\}\\=Pr\{\Omega_n>0\},\end{aligned} \tag{45}$$

where ζ_i, ξ_i and Ψ_i are as defined in (37), while Ω_n follows $\mathcal{CN}(\mu_{\Omega_n},\sigma^2_{\Omega_n})$ for $\mu_{\Omega_n}=\mu_{\Omega_p}$ and $\sigma^2_{\Omega_n}=2\kappa^2E|\varepsilon|^2+2N_0$ with:

$$\varepsilon=\sum_{i=\frac{(t-1)N}{N_t}+1}^{t\frac{N}{N_t}}\alpha_{t,i}\beta_i+\sum_{\substack{k=1\\k\neq t}}^{N_t}\sum_{i=\frac{(k-1)N}{N_t}+1}^{k\frac{N}{N_t}}\alpha_{t,i}\beta_ie^{j(\theta_{k,i}-\theta_{t,i})}. \tag{46}$$

Then, by utilizing the Q-function, the CPEP can be concluded as:

$$P_e=Q\left(\sqrt{\frac{E|\gamma|^2}{2(\kappa^2E|\varepsilon|^2+N_0)}}\right), \tag{47}$$

where γ is as defined in (40). It should be noted from (46) here that ε follows a Gaussian distribution for a large number of reflectors according to CLT. Considering this, the term $|\varepsilon|^2$ in the denominator of (47) can be replaced by its expected value, which is equal to the variance of ε, i.e., $\sigma^2_\varepsilon=\frac{N}{N_t}(N_t-\frac{\pi^2}{16})$. Now, since $|\gamma|^2$ is a linear combination of two independent central chi-squared RVs with one degree of freedom, utilizing the MGF of $|\gamma|^2$, the APEP can be calculated from:

$$\begin{aligned}\overline{P}_e=\frac{1}{\pi}\int_0^{\frac{\pi}{2}}\Bigg(&\frac{1}{\sqrt{1+\frac{NE(8-\pi^2+8N_t)}{16N_t(\kappa^2E\frac{N}{N_t}(N_t-\frac{\pi^2}{16})+N_0)\sin^2\eta}}}\\&\times\frac{1}{\sqrt{1+\frac{NE(N_t-1)}{2N_t(\kappa^2E\frac{N}{N_t}(N_t-\frac{\pi^2}{16})+N_0)\sin^2\eta}}}\Bigg)d\eta.\end{aligned} \tag{48}$$

It is worthy of noting that the APEP value is dependent neither on N nor on E for the high SNR region, since (48) can be rewritten under the assumption of $E\gg1$ as follows:

$$\begin{aligned}\overline{P}_e=\frac{1}{\pi}\int_0^{\frac{\pi}{2}}\Bigg(&\frac{1}{\sqrt{1+\frac{(8-\pi^2+8N_t)}{(16N_t-\pi^2)\kappa^2\sin^2\eta}}}\\&\times\frac{1}{\sqrt{1+\frac{8(N_t-1)}{(16N_t-\pi^2)\kappa^2\sin^2\eta}}}\Bigg)d\eta,\end{aligned} \tag{49}$$

which means that the remark provided in Section III-A-2 is valid for the partitioned RIS-SSK scheme, as well.

D. Average Bit Error Rate (ABER)

Assume that the APEP is independent of the activated Tx antennas, and thus identical for all pairs, i.e., $\overline{P}_e$ for all $(t\rightarrow\hat{t})$. The ABER value of an SSK scheme can hence be calculated in the form of a union bound [3] as follows:

$$\overline{P}_b\leq\frac{1}{\log_2N_t}\sum_{\hat{t}}\overline{P}_e\times d(t\rightarrow\hat{t})=\frac{N_t}{2}\overline{P}_e, \tag{50}$$

where $d(t\rightarrow\hat{t})$ denotes the Hamming distance between the binary representations of t and $\hat{t}$, while $\sum_{\hat{t}}d(t\rightarrow\hat{t})=(N_t/2)\log_2N_t$ for all t due to bit symmetry.

IV. Detection Complexity Analysis

In this section, we present the computational complexity of the detectors at the Rx of the proposed RIS-SSK schemes, which can be calculated by simply finding the number of real additions and real multiplications. Noting that each complex multiplication requires four real multiplications and two real additions, while the square of the absolute value of the complex number requires two real multiplications and one real addition [28]. The complexity of the RIS-SSK schemes are investigated using (2), (9) and (14).

In (2), the calculation of $\sum_{i=1}^N\alpha_{t,i}\beta_i$ requires N real multiplications as well as $(N-1)$ real summations. Multiplication of $\sqrt{E}$ accompanies a real multiplication, while subtracting $\sqrt{E}(\sum_{i=1}^N\alpha_{t,i}\beta_i)$ from y_{rp} requires a real summation. Considering also the square of the absolute value of the calculated complex value and the repetition of this process for each Tx antenna, the computational complexity of the reference scheme includes $(N+3)N_t$ multiplications and $(N+1)N_t$

TABLE I
DETECTION COMPLEXITY ANALYSIS SUMMARY

Scheme	Summation	Multiplication
Reference Int. RIS-SSK	$(N+1)N_t$	$(N+3)N_t$
Power Sensing RIS-SSK	$(N+1)N_t$	$(N+4)N_t$
Partitioned RIS-SSK	$(6N-N/N_t+1)N_t$	$(8N+4)N_t$

summations. The calculation of (9) requires implementing the same procedure with an extra multiplication for $\sqrt{k_t}$.

In (14), $(h_{t,i}e^{j\phi_{k,i}}g_i)$ can be calculated by the multiplication of three complex numbers with 8 real multiplications and 4 real summations for each reflecting element, which means this is repeated N times. Among these N multiplications, N/N_t of them provides real numbers, while the others are complex. Taking this into account, all the values are added up, and the result of the summation is multiplied by $\sqrt{E}$, and then the obtained value is subtracted from y_p. The end result is a cost of $(2N-N/N_t)$ real summations and 2 real multiplications. Considering also the square of the absolute value and the repetition of this process for each Tx antenna, the computational complexity of the partitioned scheme is calculated as $(8N+4)N_t$ multiplications and $(6N-N/N_t+1)$ summations.

The results of the complexity analysis are summarized in Table I. It is clear from this table that the partitioned scheme has the most complex detector, while the reference and power sensing scenarios have almost the same complexity. It is worth remembering here that the power sensing scheme needs some changes in the base station to be able to send the data over different power levels beside integrating sensors on the RIS. Instead, the required changes are implemented in the control software for the partitioned scheme, which is easier in practical scenarios. Therefore, it can be said that there exists a trade-off between the ease of implementation and detection complexity.

V. SIMULATION RESULTS

In this section, we present extensive Monte Carlo simulations to investigate the error performance of the proposed RIS-SSK schemes, which assumed to be fully-synchronized, considering both ideal and non-ideal transceivers. The simulations are realized by first generating a random data sequence, and then modulating them to be sent to the receiver through the RIS. Meanwhile, the modulated symbols have experienced channel and noise effects, which are characterized in accordance with their statistical model. During the simulations, at least 10^5 symbols have been sent for each SNR value, which is defined as E/N_0. Our computer simulation results, i.e., the curves of ABER versus SNR, are verified by the analytical derivations provided in Section III, and compared to the reference scheme. The effect of any large-scale path loss is ignored unless otherwise stated, since it is implicitly counted in the received SNR [3]. Lastly, N_t is assumed to be two for simplicity.

First, the effect of non-ideal transceivers is investigated for the reference intelligent RIS-SSK scheme in terms of ABER by using both the analytical derivations and computer simulations in Fig. 4. Not only is there a noticeable performance degradation but also an error floor, which is due to the non-ideal transceivers. The error floor becomes more serious with increasing levels of HWI. According to this figure, doubling the number of reflecting elements, N, enables this scheme to achieve the same ABER performance with 3 dB less SNR. However, this is not the case for the high SNR regions with HWI, since the dominant noise is not the AWGN anymore but the noise stemming from the HWI. Hence, supporting Remark 1, Fig. 4 proves the restrictive effect of the non-ideal transceivers on the overall system performance of the reference intelligent scheme, regardless of N for the high SNR region.

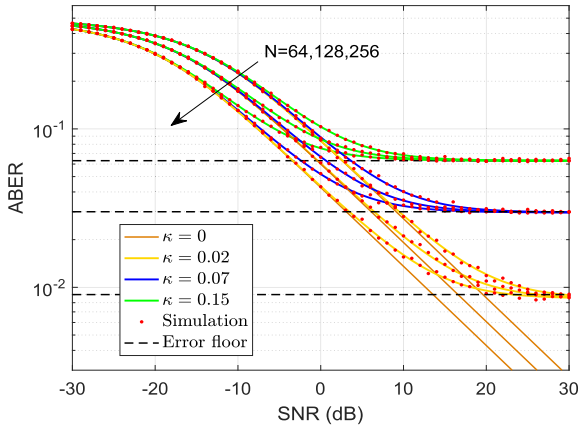

Fig. 4. The ABER performance of the reference intelligent RIS-SSK scheme with different values of κ and N.

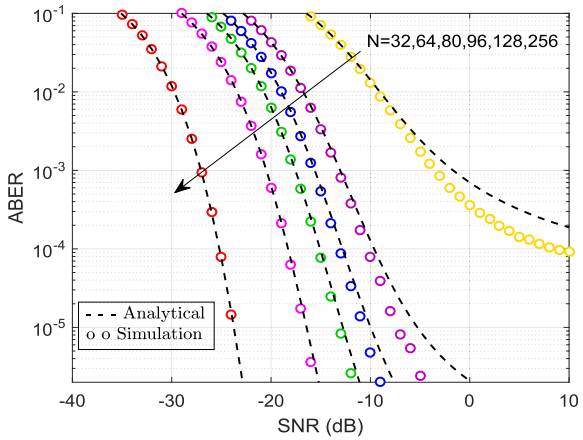

Fig. 5. The ABER performance of the power sensing RIS-SSK scheme for a fixed value of $\kappa = 0.07$ with increasing N.

Following that, the performance of the power sensing RIS-SSK scheme is presented for a fixed level of HWI, $\kappa = 0.07$, in Fig. 5. It is observed that increasing N provides a much lower ABER for a fixed value of SNR. For instance, assume that the value of SNR is -16 dB, then according to this figure, an ABER value of 6.6×10^{-3} can be achieved using a power sensing RIS-SSK scheme with 64 reflecting elements, while it decreases to 3.6×10^{-6} for $N = 128$. This figure proves that our derivations are considerably accurate, especially when $N \geq 96$, as the theoretical analyses are realized based on the CLT, which requires a sufficiently large number of reflectors to hold. The performance of the power sensing RIS-SSK scheme is also investigated in Fig. 6 with increasing values of κ by utilizing the analytical derivations in Section III-B.

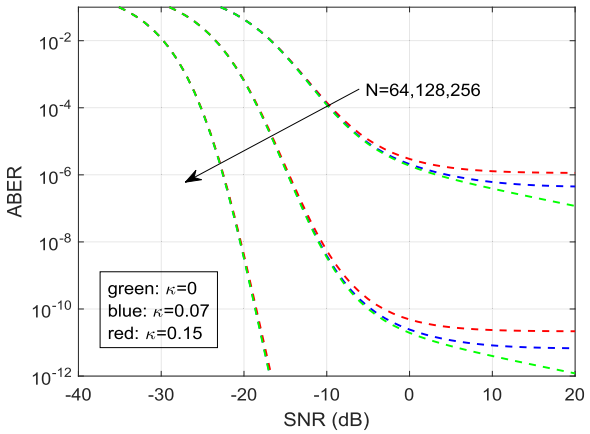

Fig. 6. The analytical ABER results of the power sensing RIS-SSK scheme for different values of κ and N.

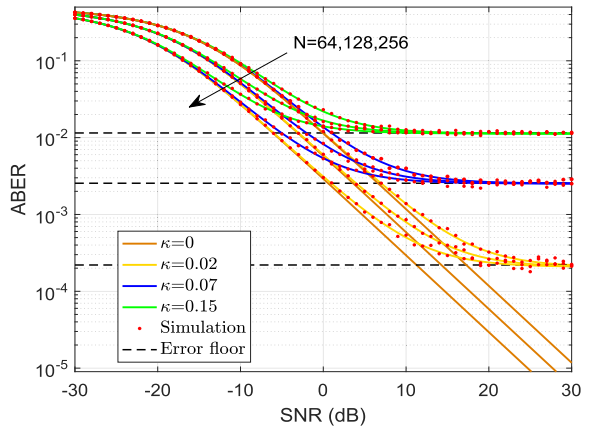

Fig. 7. The ABER performance of the partitioned RIS-SSK scheme with different values of κ and N.

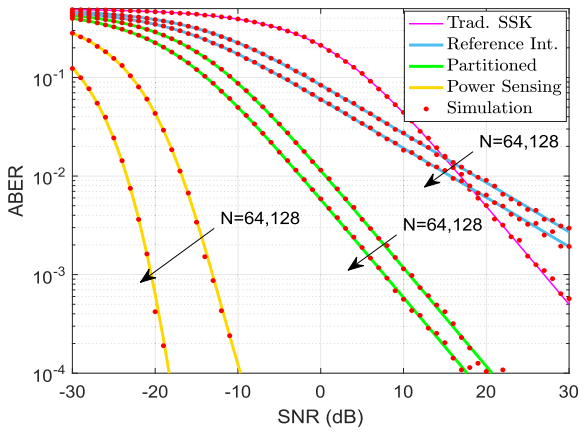

Fig. 8. Performance comparison of the proposed RIS-SSK schemes and the reference schemes under the assumption of perfect transceivers, i.e., $\kappa = 0$.

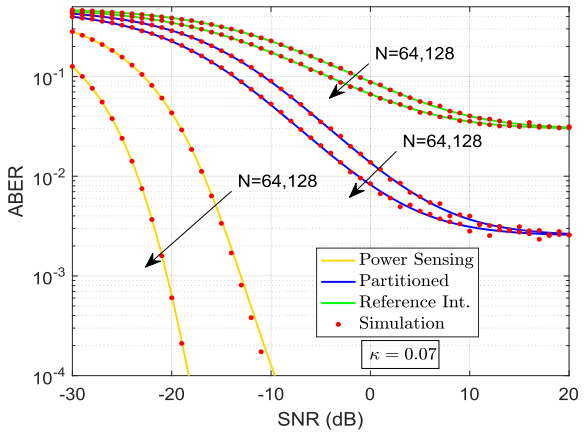

Fig. 9. Performance comparison of the intelligent, partitioned and power sensing RIS-SSK schemes under the assumption of non-ideal transceivers.

Considering both Figs. 5 and 6, it can be concluded that the detrimental impacts of the HWI can be resolved by using the power sensing RIS-SSK scheme with large values of N. It is obvious from Fig. 6 that the ABER is almost the same in case of both ideal and non-ideal hardware assumptions until a certain SNR value. Hence, there exists a trade-off between the number of reflecting elements and the required SNR for effects of the HWIs to be reasonably ignored. In other words, although an error floor is observable for the high SNR region, the achieved ABER for high N values are satisfying enough to ignore the impact of the HWI at unconventionally low SNR values. It is worth noting that all the presented results in both figures are consistent with Remark 2.

In Fig. 7, the system performance of the partitioned RIS-SSK is presented for various values of κ and N. The obtained results show that the partitioned RIS-SSK has an ABER characteristic to the reference scheme, and all the notes made regarding Fig. 4 are also valid for Fig. 7. However, it should also be highlighted that the partitioning approximation clearly offers a better quality of service.

Then, the ABER performance of the proposed RIS-SSK schemes is compared to the traditional SSK [29] under the assumption of ideal hardware in Fig. 8. In order to present objective results, traditional SSK is also assumed to be realized between two Tx antennas and one Rx antenna. As illustrated in Fig. 8, the reference scheme needs much more than 128 reflecting elements to be advantageous compared to the traditional SSK in high SNR region. On the other hand, the partitioned and power sensing schemes have results that are greatly superior to both the traditional SSK and the reference RIS-SSK for all SNR values. Obviously, the best results are obtained with the power sensing scheme, which achieves very low error rates with unconventionally high energy efficiency.

Next, the ABER performance of the intelligent, partitioned and power sensing RIS-SSK schemes is compared under the assumption of non-ideal transceivers in Fig. 9. Comparing Figs. 8 and 9, it can be concluded that the effects of the HWI have been successfully eliminated for the considered SNR region with the power-sensing scheme, while an error floor is observable in the ABER performance of the other schemes. Clearly, the presented results in both figures are consistent with the provided discussions regarding Figs. 4-8.

Fig. 10 investigates the effect of path loss on the proposed RIS-SSK schemes by assuming that the overall system path loss is $(\lambda^2/16\pi d_1 d_2)^2$ [30], where λ is the wavelength for an operating frequency of 2.4 GHz, while d_1 and d_2 are the distances between the Tx-RIS and RIS-Rx, respectively. This investigation involves varying d_1 for $d = d_1 + d_2 = 10$ and $N = 128$. It is shown that a better ABER occurs when the RIS is close to the Tx. Indeed, a similar result can be expected

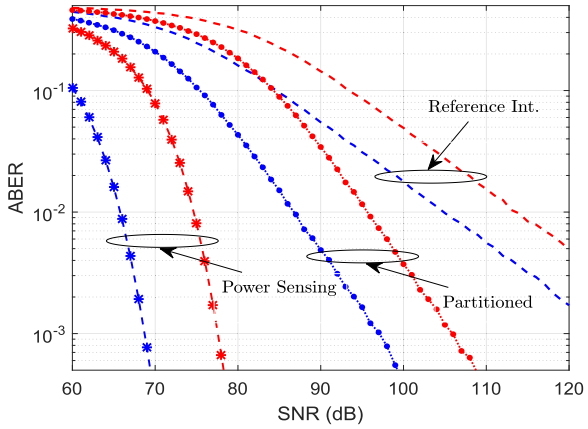

Fig. 10. The effect of path loss on the proposed RIS-SSK schemes with perfect transceivers, i.e., $\kappa = 0$ (blue: $d_1 = 1$ m, $d_2 = 9$ m; red: $d_1 = d_2 = 5$ m).

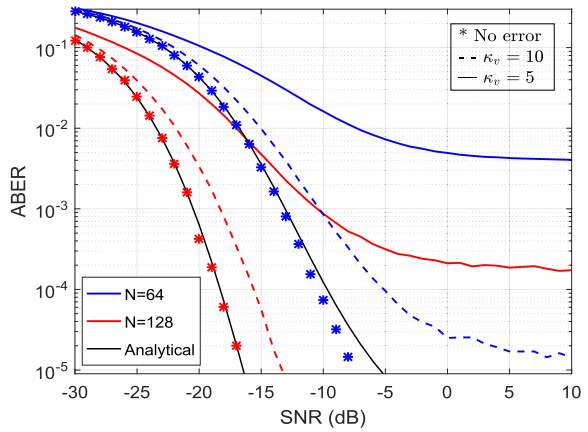

Fig. 11. The ABER performance of the power sensing RIS-SSK scheme with perfect transceiver in the presence of phase estimation error at the RIS.

when the RIS is close to the Rx for a fixed d by considering the path loss expression. Comparing Figs. 8 and 10, it can be concluded that the path loss has a very serious destructive effect on all schemes.

Lastly, the performance of the power sensing RIS-SSK scheme in the presence of channel phase estimation errors at the RIS is indicated in Fig. 11. For this, the phase error, ϑ_i, is modelled as a zero-mean von Mises variable with a concentration parameter κ_v that captures the accuracy of the estimation [4], [31], since the residual phase errors of phase trackers follow von Mises distribution [32]. Then, the reflection phases are specified by taking the phase error into account as $\phi_{t,i} = \theta_{t,i} + \psi_i + \vartheta_i$. As can be seen from this figure, the knowledge of the channel phases is crucial to the overall system performance of the power sensing RIS-SSK. For instance, when $N = 128$, the deviation from perfect channel phase information is about 2-3 dB while $\kappa_v = 10$ (more accurate estimation). However, while $\kappa_v = 5$ (for which the distribution is broad) an error floor occurs at ABER $= 2 \times 10^{-4}$ in the positive SNR region.

VI. Conclusion

This paper presented a framework for future RIS-assisted SSK systems as well as two applicable transmission schemes. Theoretical derivations were presented by using ML detectors for the calculation of the ABER, and extensive computer simulation results were provided to assess the potential of the proposed systems. Moreover, the existence of non-ideal transceivers has been considered as a case study. Noting that the data is conveyed through the activated channels in SSK, it needs a rich scattering environment to achieve a good performance, which highly depends on the distinctness of the channels. Regarding this, it was observed that cancelling all the channel phases in the reference scheme through the RIS reduces the differences between the channels, which means limiting the performance of the SSK. This restriction is resolved by partitioning and power sensing approximations, which underlies the novel RIS-SSK schemes proposed in this study. Although the partitioned RIS-SSK has a much more complex detection procedure compared to the others, the power sensing RIS-SSK provides a highly reliable transmission and unconventionally high energy efficiency with almost no additional cost of complexity, even in the case of non-ideal transceivers. The perfect match between the presented analytical and simulation results verifies the accuracy of the provided theoretical derivations. Importantly, the effects of path loss should be taken into account carefully for the future wireless communication networks. Since the knowledge of the channel phases at the RIS is crucial, an interesting future research direction can be the development of new, possibly deep learning-based, algorithms for RIS-assisted SSK systems. Besides, the case of imperfect channel state information at the Rx side can also be investigated.

References

[1] M. Xiao *et al.*, "Millimeter wave communications for future mobile networks," *IEEE J. Sel. Areas Commun.*, vol. 35, no. 9, pp. 1909–1935, Sep. 2017.

[2] T. Mao, Q. Wang, Z. Wang, and S. Chen, "Novel index modulation techniques: A survey," *IEEE Commun. Surveys Tuts.*, vol. 21, no. 1, pp. 315–348, 1st Quart., 2018.

[3] E. Basar, "Reconfigurable intelligent surface-based index modulation: A new beyond MIMO paradigm for 6G," *IEEE Trans. Commun.*, vol. 68, no. 5, pp. 3187–3196, May 2020.

[4] A. E. Canbilen, E. Basar, and S. S. Ikki, "Reconfigurable intelligent surface-assisted space shift keying," *IEEE Wireless Commun. Lett.*, vol. 9, no. 9, pp. 1495–1499, Sep. 2020.

[5] J. Yuan, M. Wen, Q. Li, E. Basar, G. C. Alexandropoulos, and G. Chen, "Receive quadrature reflecting modulation for RIS-empowered wireless communications," *IEEE Trans. Veh. Technol.*, vol. 70, no. 5, pp. 5121–5125, May 2021.

[6] S. Lin, M. Wen, M. Di Renzo, and F. Chen, "Reconfigurable intelligent surface-based quadrature reflection modulation," in *Proc. IEEE Int. Conf. Commun. (ICC)*, Jun. 2021, pp. 1–6.

[7] Q. Li, M. Wen, S. Wang, G. C. Alexandropoulos, and Y.-C. Wu, "Space shift keying with reconfigurable intelligent surfaces: Phase configuration designs and performance analysis," *IEEE Open J. Commun. Soc.*, vol. 2, pp. 322–333, 2021.

[8] A. Bhowal, S. Aissa, and R. S. Kshetrimayum, "RIS-assisted advanced spatial modulation techniques for ambient backscattering communications," *IEEE Trans. Green Commun. Netw.*, vol. 5, no. 4, pp. 1684–1696, Dec. 2021.

[9] S. Luo *et al.*, "Spatial modulation for RIS-assisted uplink communication: Joint power allocation and passive beamforming design," *IEEE Trans. Commun.*, vol. 69, no. 10, pp. 7017–7031, Oct. 2021.

[10] C. Studer, M. Wenk, and A. Burg, "MIMO transmission with residual transmit-RF impairments," in *Proc. Int. ITG Workshop Smart Antennas (WSA)*, Feb. 2010, pp. 189–196.

[11] Z. Xing, R. Wang, J. Wu, and E. Liu, "Achievable rate analysis and phase shift optimization on intelligent reflecting surface with hardware impairments," *IEEE Trans. Wireless Commun.*, vol. 20, no. 9, pp. 5514–5530, Sep. 2021.

[12] A. Afana and S. Ikki, "Analytical framework for space shift keying MIMO systems with hardware impairments and co-channel interference," *IEEE Commun. Lett.*, vol. 21, no. 3, pp. 488–491, Mar. 2017.
[13] A. E. Canbilen, S. S. Ikki, E. Basar, S. S. Gultekin, and I. Develi, "Joint impact of I/Q imbalance and imperfect CSI on SM-MIMO systems over generalized Beckmann fading channels: Optimal detection and Cramer-Rao bound," *IEEE Trans. Wireless Commun.*, vol. 19, no. 5, pp. 3034–3046, May 2020.
[14] M. M. Alsmadi, A. E. Canbilen, N. A. Ali, and S. S. Ikki, "Effect of generalized improper Gaussian noise and in-phase/quadrature-phase imbalance on quadrature spatial modulation," *IEEE Open J. Signal Process.*, vol. 2, pp. 295–308, 2021.
[15] T. Mao, Q. Wang, and Z. Wang, "Spatial modulation for terahertz communication systems with hardware impairments," *IEEE Trans. Veh. Technol.*, vol. 69, no. 4, pp. 4553–4557, Apr. 2020.
[16] A.-A.-A. Boulogeorgos and A. Alexiou, "How much do hardware imperfections affect the performance of reconfigurable intelligent surface-assisted systems?" *IEEE Open J. Commun. Soc.*, vol. 1, pp. 1185–1195, 2020.
[17] S. Zhou, W. Xu, K. Wang, M. Di Renzo, and M.-S. Alouini, "Spectral and energy efficiency of IRS-assisted MISO communication with hardware impairments," *IEEE Wireless Commun. Lett.*, vol. 9, no. 9, pp. 1366–1369, Sep. 2020.
[18] E. Saleh, M. M. Alsmadi, A. Bouhlel, A. E. Canbilen, N. A. Ali, and S. Ikki, "Impact of channel correlation and hardware impairments on large intelligent surfaces-aided communication systems," in *Proc. IEEE 32nd Annu. Int. Symp. Pers., Indoor Mobile Radio Commun. (PIMRC)*, Sep. 2021, pp. 805–810.
[19] M. H. N. Shaikh, V. A. Bohara, A. Srivastava, and G. Ghatak, "Performance analysis of intelligent reflecting surface-assisted wireless system with non-ideal transceiver," *IEEE Open J. Commun. Soc.*, vol. 2, pp. 671–686, 2021.
[20] K. Zhi, C. Pan, H. Ren, and K. Wang, "Uplink achievable rate of intelligent reflecting surface-aided millimeter-wave communications with low-resolution ADC and phase noise," *IEEE Wireless Commun. Lett.*, vol. 10, no. 3, pp. 654–658, Mar. 2021.
[21] A. Bouhlel, M. M. Alsmadi, E. Saleh, S. Ikki, and A. Sakly, "Performance analysis of RIS-SSK in the presence of hardware impairments," in *Proc. IEEE 32nd Annu. Int. Symp. Pers., Indoor Mobile Radio Commun. (PIMRC)*, Sep. 2021, pp. 537–542.
[22] A. E. Canbilen, "Performance analysis of RIS-assisted SM with I/Q imbalance," *Phys. Commun.*, vol. 49, Dec. 2021, Art. no. 101473.
[23] Z. Yigit, E. Basar, and I. Altunbas, "Low complexity adaptation for reconfigurable intelligent surface-based MIMO systems," *IEEE Commun. Lett.*, vol. 24, no. 12, pp. 2946–2950, Dec. 2020.
[24] A. Pizzo, T. L. Marzetta, and L. Sanguinetti, "Spatially-stationary model for holographic MIMO small-scale fading," *IEEE J. Sel. Areas Commun.*, vol. 38, no. 9, pp. 1964–1979, Sep. 2020.
[25] M. Matthaiou, A. Papadogiannis, E. Björnson, and M. Debbah, "Two-way relaying under the presence of relay transceiver hardware impairments," *IEEE Commun. Lett.*, vol. 17, no. 6, pp. 1136–1139, Jun. 2013.
[26] E. Björnson, J. Hoydis, and L. Sanguinetti, "Massive MIMO networks: Spectral, energy and hardware efficiency," *Found. Trends Signal Process.*, vol. 11, nos. 3–4, pp. 154–655, Nov. 2017.
[27] L. Subrt and P. Pechac, "Controlling propagation environments using intelligent walls," in *Proc. 6th Eur. Conf. Antennas Propag. (EUCAP)*, Mar. 2012, pp. 1–5.
[28] M. M. Alsmadi, A. E. Canbilen, N. Abu Ali, S. S. Ikki, and E. Basar, "Cognitive networks in the presence of I/Q imbalance and imperfect CSI: Receiver design and performance analysis," *IEEE Access*, vol. 7, pp. 49765–49777, 2019.
[29] J. Jeganathan, A. Ghrayeb, L. Szczecinski, and A. Ceron, "Space shift keying modulation for MIMO channels," *IEEE Trans. Wireless Commun.*, vol. 8, no. 7, pp. 3692–3703, Jul. 2009.
[30] I. Al-Nahhal, O. A. Dobre, E. Basar, T. M. N. Ngatched, and S. Ikki, "Reconfigurable intelligent surface optimization for uplink sparse code multiple access," *IEEE Commun. Lett.*, vol. 26, no. 1, pp. 133–137, Jan. 2022.
[31] A. Papazafeiropoulos, C. Pan, P. Kourtessis, S. Chatzinotas, and J. M. Senior, "Intelligent reflecting surface-assisted MU-MISO systems with imperfect hardware: Channel estimation and beamforming design," *IEEE Trans. Wireless Commun.*, vol. 21, no. 3, pp. 2077–2092, Mar. 2022.
[32] M. Badiu and J. P. Coon, "Communication through a large reflecting surface with phase errors," *IEEE Wireless Commun. Lett.*, vol. 9, no. 2, pp. 184–188, Feb. 2020.

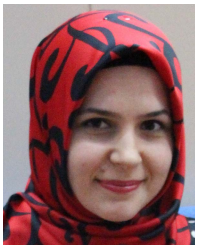

Ayse E. Canbilen (Member, IEEE) received the Ph.D. degree from Konya Technical University in 2019. From 2017 to 2018, she was with the Department of Electrical Engineering, Lakehead University, Thunder Bay, ON, Canada, as a Visitor Researcher. She is currently an Assistant Professor with the Department of Electrical and Electronics Engineering, Konya Technical University, Konya, Turkey. Her primary research interests include beyond 5G systems, spatial modulation techniques, reconfigurable intelligent surfaces, and visible light communications. She has been serving as a Reviewer of the IEEE TRANSACTIONS ON COMMUNICATIONS, IEEE TRANSACTIONS ON WIRELESS COMMUNICATIONS, IEEE TRANSACTIONS ON VEHICULAR TECHNOLOGY, IEEE COMMUNICATIONS LETTERS, and IEEE ACCESS.

Ertugrul Basar (Senior Member, IEEE) received the Ph.D. degree from Istanbul Technical University in 2013. He has been the Director of the Communications Research and Innovation Laboratory (CoreLab) since 2018. He is currently an Associate Professor with the Department of Electrical and Electronics Engineering, Koç University, Istanbul, Turkey. His primary research interests include beyond 5G systems, index modulation, intelligent surfaces, waveform design, and deep learning/signal processing for communications. He currently serves as a Senior Editor of IEEE COMMUNICATIONS LETTERS and an Editor of IEEE TRANSACTIONS ON COMMUNICATIONS and FRONTIERS IN COMMUNICATIONS AND NETWORKS. He is a Young Member of the Turkish Academy of Sciences. He is the Founding Academic Chair of the IEEE ComSoc Emerging Technologies Initiative on Reconfigurable Intelligent Surfaces.

Salama S. Ikki (Senior Member, IEEE) was a Visiting Research Professor (Nokia Scholarship) at Aalto University, Helsinki, Finland, in 2022. He is currently an Associate Professor and the Research Chair of Wireless Communications with Lakehead University, Thunder Bay, ON, Canada. His research group has made substantial contributions to 4G and 5G wireless technologies. He is the author of more than 100 journals and conference papers and has more than 5500 citations and an H-index of 35. His group's current focuses on massive MIMO, cell-free massive MIMO, visible light communications, and wireless sensor networks. He received several awards for his research, teaching, and services.